catalysts

MDPI

Article

Facile Preparation of a Novel Bi_2WO_6/Calcined Mussel Shell Composite Photocatalyst with Enhanced Photocatalytic Performance

Shijie Li [1,*], Chunchun Wang [1,2], Yanping Liu [1,2,*], Bing Xue [1,2], Jialin Chen [1,2], Hengwei Wang [1] and Yu Liu [1]

[1] Key Laboratory of Health Risk Factors for Seafood of Zhejiang Province, National Engineering Research Center for Marine Aquaculture, Institute of Innovation & Application, Zhejiang Ocean University, Zhoushan 316022, Zhejiang, China; wcc14nb@126.com (C.W.); xb1725621827@163.com (B.X.); chenjialin_haihua@163.com (J.C.); wanghw@zjou.edu.cn (H.W.); liuyu1987@zjou.edu.cn (Y.L.)

[2] College of Marine Science and Technology, Zhejiang Ocean University, Zhoushan 316022, Zhejiang, China

* Correspondence: lishijie@zjou.edu.cn (S.L.); liuyp@zjou.edu.cn (Y.L.); Tel.: +86-21-67792557 (S.L.)

Received: 15 September 2020; Accepted: 4 October 2020; Published: 12 October 2020

Abstract: The exploration of cost-effective and highly efficient photocatalysts is still a great challenge. In this work, a cost-effective and highly active Bi_2WO_6/calcined mussel shell (CMS/BWO) composite photocatalyst was prepared by a facile solvothermal route, in which Bi_2WO_6 nanosheets were tightly, evenly, and vertically grown on waste calcined mussel shells (CMS). Multiple techniques are adopted to characterize the phases, morphology, and chemical properties of the as-fabricated catalysts. In contrast to the stacked Bi_2WO_6, CMS/BWO has numerous exposed edges and open transfer pathways, which can create more open space and reactive sites for photocatalytic reactions. Such favorable characteristics enable CMS/BWO to efficiently degrade organic pollutants (e.g., rhodamine B (RhB), methylene blue (MB), tetracycline hydrochloride (TC)) under visible light. Moreover, the generation of reactive species during the photocatalytic process is also examined by trapping experiments, disclosing the pivotal role of photo-generated holes (h^+) and hydroxyl radicals (•OH) in the photo-degradation of pollutants. Above all, this study not only provides an efficient photocatalyst for environmental remediation, but it also opens up new possibilities for waste mussel shell reutilization.

Keywords: mussel shell; Bi_2WO_6; visible-light photocatalysis; pollutant degradation; waste mussel shell reutilization

1. Introduction

Refractory organic pollutants, such as industrial dyes and antibiotics, bring a huge threat to the environment. How to effectively remove these pollutants has been one of the most concerning topics in the field of environmental remediation. Several means have been employed to remove pollutants, including adsorption, biological degradation, and chemical oxidation [1–3]. Among them, a semiconductor-based photocatalysis technique, which deploys sunlight for the effective decomposition of pollutants, has drawn worldwide interest due to its low cost, high efficiency, and sustainability [4]. In light of the actual application, great efforts have been contributed to the exploration of excellent photocatalysts [5–19].

Among numerous potential photocatalysts, one of the Bi-based compounds, bismuth tungstate (Bi_2WO_6) with unique layer structures, high chemical stability, and good optical properties, is considered

as a promising visible-light-driven (VLD) photocatalyst for photocatalytic elimination of pollutants [20–22]. However, the unsatisfactory photocatalytic performance hinders the practical application in wastewater purification. To improve its photocatalytic performance, various strategies have been adopted, such as morphology control [23], doping [24], metal deposition [25], and heterojunction formation [26–29]. However, these materials usually suffer from a high cost and complicated preparation procedure.

Mussel shells, as a primary by-product of the mussel aquaculture industry, are a kind of abundant natural resource and commonly abandoned as waste. A huge number of mussel shells are disposed of in landfills or seawater, causing environmental pollution. Actually, mussel shells, mainly composed of calcium carbonate, can be an important resource for the preparation of value-added products by virtue of their intrinsic characteristics. As is known, shells are an abundant biomass material with a special multi-scale and multi-level "brick-mud" assembly structure. Up to now, mussel shells have been utilized to remove heavy metals in mine soil [30]. Meanwhile, they can be employed to improve the photocatalytic performance of catalysts [31–33]. Consequently, constructing Bi_2WO_6/calcined mussel shell composites should be an appealing strategy for the promotion of photocatalytic performance towards organic pollutants.

Herein, hierarchical Bi_2WO_6/calcined mussel shell (CMS/BWO) composites were prepared via a facile solvothermal route. Three pollutants (rhodamine B (RhB), tetracycline hydrochloride (TC), and methylene blue (MB)) were selected as models to investigate the degradation performance of the CMS/BWO composite under visible light irradiation. The stability and mineralization capability of CMS/BWO were also studied. A plausible photocatalytic mechanism was also proposed.

2. Results and Discussion

2.1. Phase and Microstructure

The crystalline phases of the samples were examined by powder X-ray diffraction (XRD) analysis, and the results are presented in Figure 1. For bare Bi_2WO_6, the main diffraction peaks were well-matched with the orthorhombic Bi_2WO_6 phase (Joint Committee on Powder Diffraction Standards, JCPDS 73-1126) [27]. Meanwhile, the XRD pattern of calcined mussel shells (CMS) revealed that CMS is composed of a calcite type of $CaCO_3$ (JCPDS 83-1762) and the hexagonal phase of $Ca(OH)_2$ (JCPDS 04-0733). The presence of $Ca(OH)_2$ is probably due to the fact that $CaCO_3$ is decomposed into CaO at a high temperature, which further reacts with H_2O to generate $Ca(OH)_2$. As for the Bi_2WO_6/calcined mussel shell (CMS/BWO-1, 2, 3) composites, the XRD patterns of CMS/BWO-1 and CMS/BWO-2 only showed the diffraction peaks of Bi_2WO_6, probably due to the low content of CMS in the composite. By contrast, the XRD pattern of CMS/BWO-3 displayed a new peak at $2\theta = 29.2°$, which could be attributed to the (104) plane of the calcite type of $CaCO_3$ (JCPDS 83-1762). Additionally, no other peaks from impurities were identified in the XRD patterns, reflecting that the CMS/BWO composites were successfully prepared.

Scanning electron microscopy (SEM) was employed to visualize the microstructure of Bi_2WO_6 and the Bi_2WO_6/calcined mussel shell composite (CMS/BWO-2). CMS showed nano-flake morphology with differently sized pores caused by organics escaping from the shells after a high-temperature treatment (Figure 2a). Bare Bi_2WO_6 presented an agglomerate structure, which is composed of numerous stacked 2D nanosheets (Figure 2b,c). After the solvothermal reaction, the obtained CMS/BWO-2 exhibited a unique hierarchical structure, where 2D Bi_2WO_6 nanosheets were evenly and vertically anchored on the surface of CMS (Figure 2d). This fact demonstrated the successful preparation of the hierarchical Bi_2WO_6/calcined mussel shell composite, with close contact between Bi_2WO_6 and CMS.

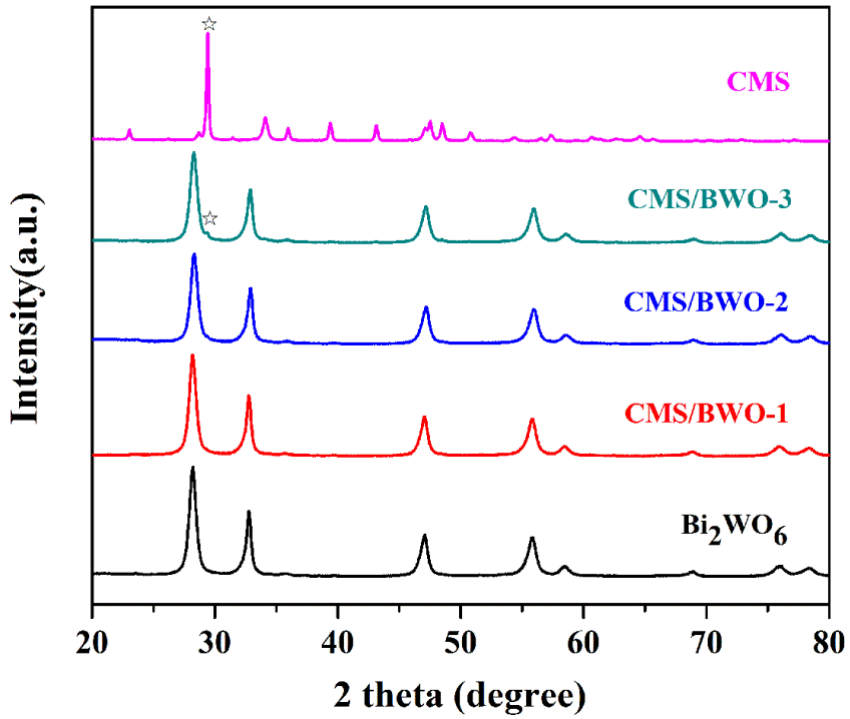

Figure 1. Powder X-ray diffraction (XRD) patterns of Bi_2WO_6, calcined mussel shells (CMS), and a series of Bi_2WO_6/calcined mussel shell (CMS/BWO-1, 2, 3) composites.

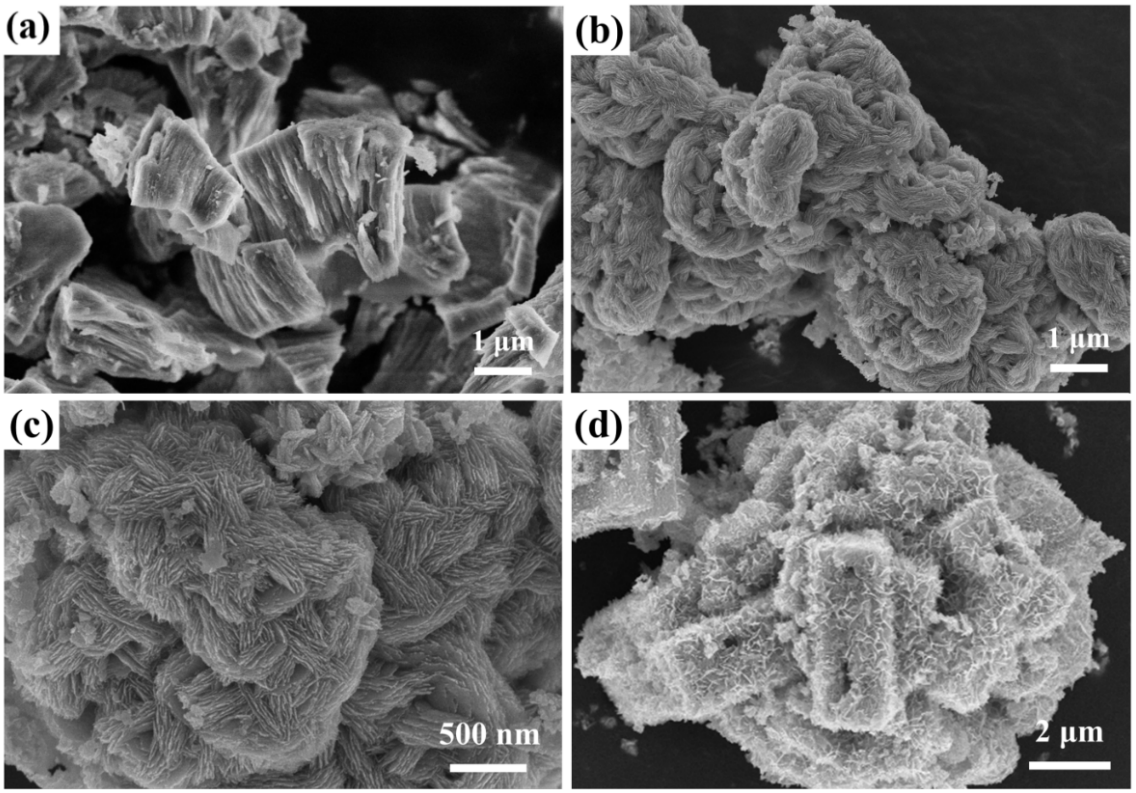

Figure 2. Scanning electron microscopy (SEM) images of calcined mussel shell (CMS) (**a**), Bi_2WO_6 (**b**,**c**), and CMS/BWO-2 (**d**).

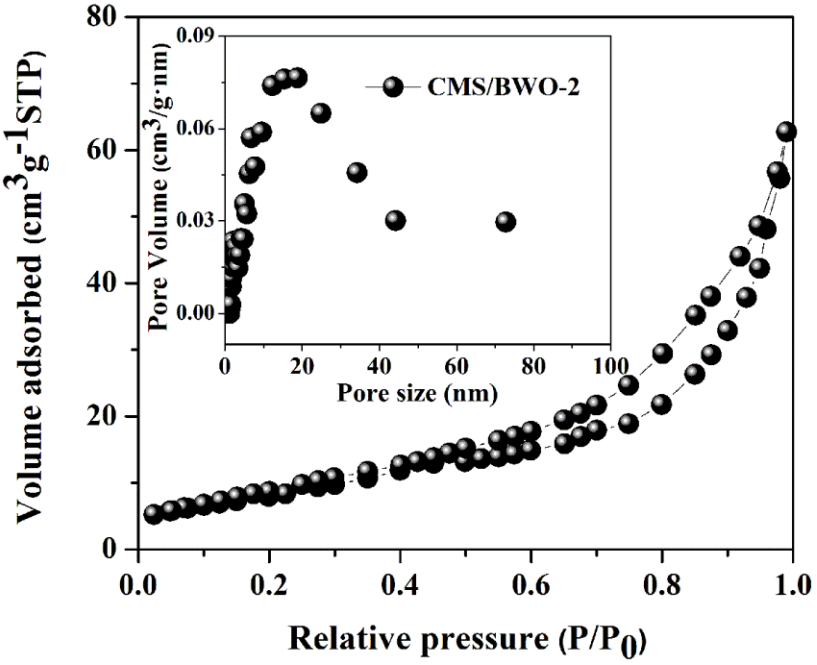

Figure 3. N_2 adsorption–desorption isotherms and the pore size distribution curves (inset) of CMS/BWO-2.

2.2. Optical Properties

UV-Vis diffuse reflection spectra (DRS) was investigated to assess the optical properties of Bi_2WO_6, CMS, and Bi_2WO_6/calcined mussel shell (CMS/BWO-1, 2, 3) composites (Figure 4a). Bi_2WO_6 displayed an intense optical absorbance in the visible light region ending at ~470.0 nm [22,34]. Noticeably, the obtained CMS/BWO composites also manifested strong absorbance in the visible light region, indicating that these composites can be anticipated to be active VLD photocatalysts. Furthermore, the band gap (E_g) of Bi_2WO_6 and CMS/BWO composites could be determined by using the Kubelka–Munk formula:

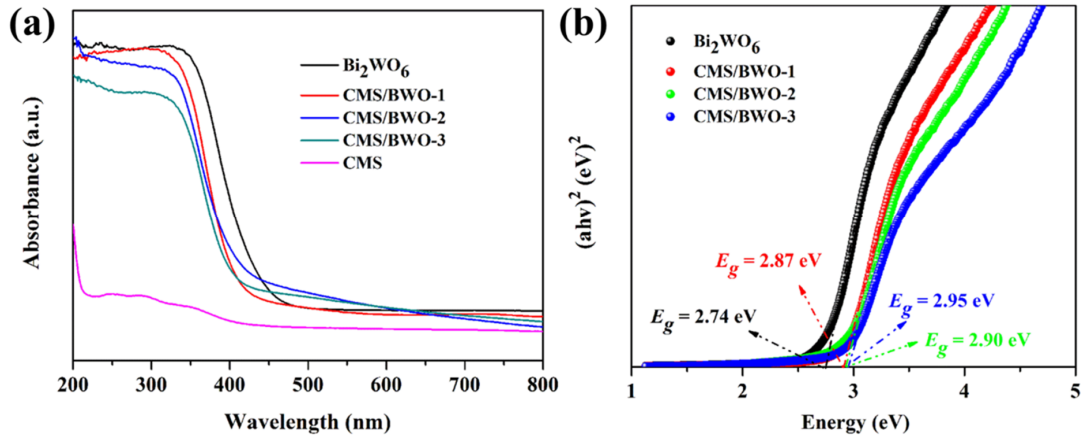

Figure 4. (**a**) UV-Vis diffuse reflection spectra (DRS) of Bi_2WO_6, CMS, calcined mussel shell (CMS), and a series of Bi_2WO_6/calcined mussel shell (CMS/BWO-1, 2, 3) composites; (**b**) plot of the $(\alpha h\upsilon)^{1/2}$ versus $h\upsilon$ for Bi_2WO_6, and the CMS/BWO composites.

$$\alpha h\nu = A(h\nu - E_g)^{n/2} \quad (1)$$

Figure 4b displays a Tauc's E_g plot of Bi_2WO_6 and CMS/BWO composites. The E_g values of the Bi_2WO_6 and CMS/BWO composites were determined to be 2.74, 2.87, 2.90, and 2.95 eV, respectively.

2.3. Photocatalytic Activity

The RhB degradation test under visible light was performed to assess the photocatalytic capability of the as-prepared catalysts (Figure 5). Figure 5a presents the RhB degradation curves over different samples. The blank test revealed that RhB showed good stability in the absence of catalysts, and almost no RhB was degraded under visible light irradiation. Bare CMS could remove 16.9% of RhB within 150 min, implying that CMS has photocatalytic activity against RhB dye. Pristine Bi_2WO_6 could degrade 73.2% of RhB within 150 min. After rationally integrating Bi_2WO_6 and CMS into hierarchical composites, the obtained CMS/BWO composites exhibited superior activity than bare CMS and Bi_2WO_6. It can be perceived that 77.4%, 98.4%, and 83.5% of RhB was removed by CMS/BWO composites with various contents of CMS. Notably, CMS/BWO-2 demonstrated to be the most active catalyst among all the tested samples. This fact indicated that a smart combination of Bi_2WO_6 and CMS could lead to the improvement of photocatalytic performance due to the following reasons: the novel hierarchical heterostructure of the composite with numerous pores could offer plenty of active sites and diffusion/transport paths, beneficial for catalytic reactions [22]; distinct from stacked Bi_2WO_6, CMS/BWO has plenty of exposed edges and open diffusion channels, offering open space and more active sites for pollutant degradation; beyond that, mussel shells contain some transition metal elements, which could improve the photocatalytic activity [31].

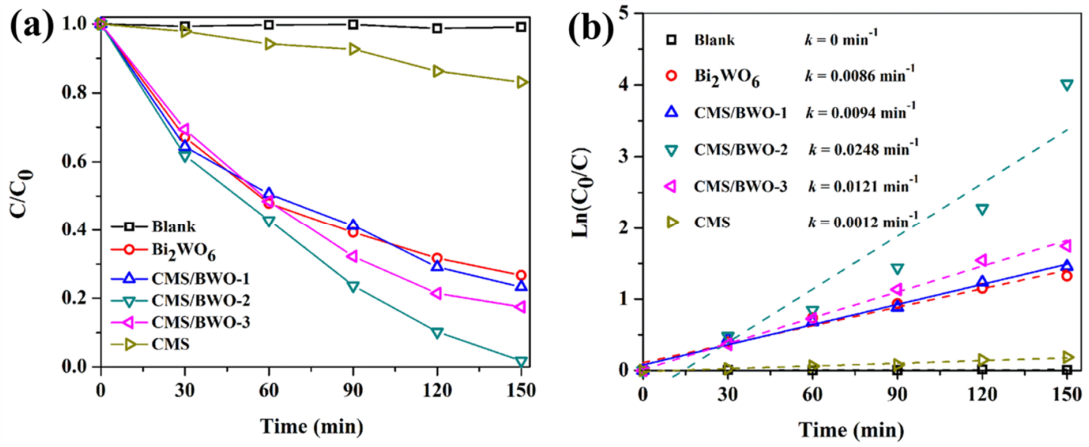

Figure 5. (**a**) Rhodamine B (RhB) (20.0 mg/L, 100.0 mL) removal curves and (**b**) the corresponding rate constant (k) of RhB degradation by the as-fabricated samples under visible light.

Furthermore, the reaction rate was estimated through the first-order kinetic equation,

$$\mathrm{Ln}(C_0/C) = kt$$

Here C_0, C, k, and t represent the initial concentration of RhB, the concentration of RhB at reaction time t, the reaction rate constant, and reaction time, respectively. As illustrated in Figure 5b, the degradation rate constants (k) for pure CMS, Bi_2WO_6, CMS/BWO-1, CMS/BWO-2, and CMS/BWO-3 were calculated to be 0.0012, 0.0086, 0.0094, 0.0248, and 0.0121 min^{-1}, respectively. Of note, CMS/BWO-2 obtained the highest k, about 2.89- and 20.06-fold as high as that of Bi_2WO_6 or CMS.

To further validate its strong photocatalytic activity, degradation of MB and TC over CMS/BWO-2 was further performed, respectively (Figure 6). After 150 min of visible light irradiation, 100% of MB and 78.4% of TC were eliminated, demonstrating its remarkable photocatalytic capability for the removal of toxic organic pollutants (RhB, MB, and TC).

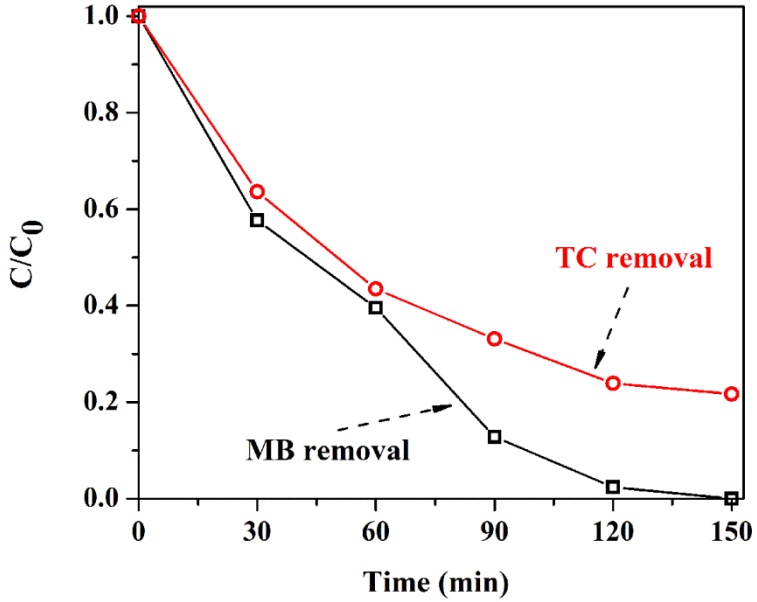

Figure 6. Methylene blue (MB) (20.0 mg/L, 100.0 mL) and tetracycline hydrochloride (TC) (20.0 mg/L, 100.0 mL) degradation curves over the Bi_2WO_6/CMS-2 composite.

For assessing the mineralization ability of CMS/BWO-2, total organic carbon (TOC) measurements were implemented. As plotted in Figure 7, the RhB was gradually mineralized with an increase of reaction time, and about 52.3% of TOC was removed after 150 min of reaction, revealing that CMS/BWO-2 could effectively mineralize the RhB pollutant.

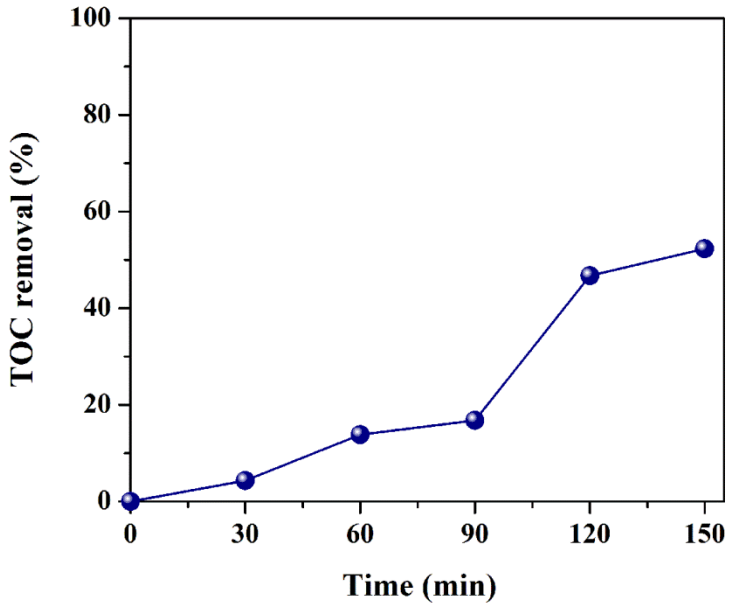

Figure 7. Total organic carbon (TOC) removal of RhB solution over CMS/BWO-2.

On account of the significance of stability and reusability for the pragmatic application of photocatalysts, cycling degradation of RhB over CMS/BWO-2 was conducted. As shown in Figure 8a, CMS/BWO-2 did not present significant deactivation, and approximately of 89.3% of RhB could be degraded even in the fifth run. The slight deterioration in the photocatalytic activity probably stemmed from the unavoidable loss of the catalyst in the experiment. Furthermore, good stability was further verified by using the XRD technique. Clearly, the phase of the used CMS/BWO-2 was almost identical

to that of the original one (Figure 8b). The above findings disclosed that CMS/BWO-2 belongs to a type of stable VLD photocatalyst, which could be a potential candidate for actual wastewater treatment.

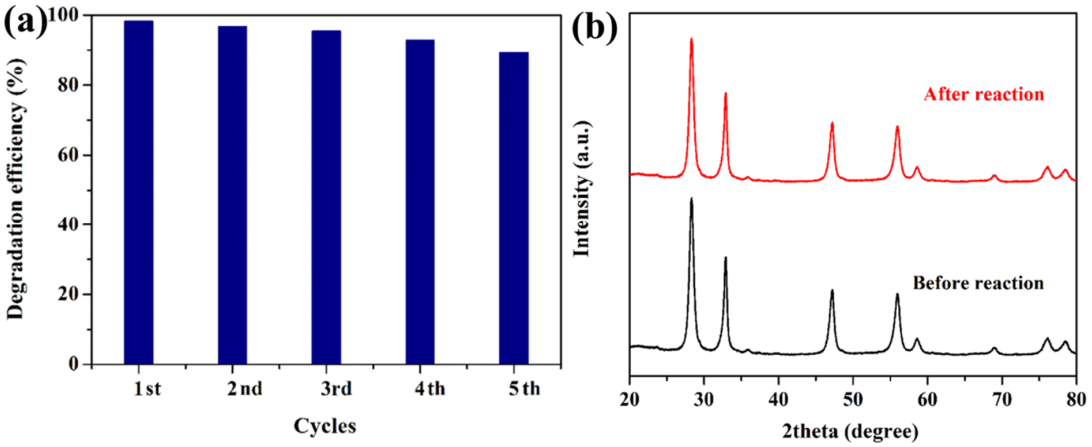

Figure 8. (**a**) Five recycling runs of CMS/BWO-2 for RhB removal; (**b**) the XRD patterns of the original and recycled CMS/BWO-2.

2.4. Photocatalytic Mechanism

The photocatalytic mechanism of CMS/BWO-2 composite for the degradation of RhB was studied by active species trapping experiments. 4-hydroxy-2, 2, 6, 6-tetramethylpiperidine-N-oxyl (TEMPOL), isopropanol (IPA), and ammonium oxalate (AO) were employed as the quenchers of $\bullet O_2^-$, hydroxyl radicals (•OH), and photo-generated holes (h^+), respectively [35]. Figure 9 displays the degradation efficiency of RhB over CMS/BWO-2 in the presence of various quenchers. The introduction of IPA and AO significantly suppressed the photocatalytic activity of CMS/BWO-2 and made the RhB degradation efficiency drop sharply from 98.4% to 29.7% and 58.4%, respectively. By contrast, the addition of TEMPOL only slightly impacted the degradation of RhB. Clearly, the contributory role of reactive species followed the order $\bullet OH > h^+ > \bullet O_2^-$. This fact demonstrated that •OH and h^+ species played a pivotal role in the degradation of RhB.

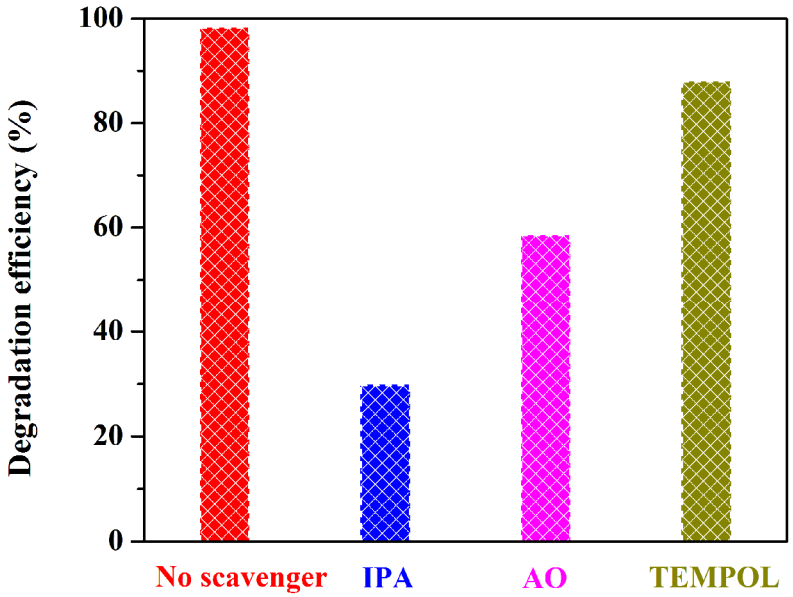

Figure 9. Active species quenching experiments.4-hydroxy-2, 2, 6, 6-tetramethylpiperidine-N-oxyl (TEMPOL), isopropanol (IPA), and ammonium oxalate (AO).

The proposed photocatalytic mechanism for the effective degradation of pollutants over the CMS/BWO composite photocatalyst is displayed in Figure 10. The novel hierarchical structure of CMS/BWO was conducive to improving the photocatalytic behavior with virtues of a high specific surface area, sufficient reactive sites, and rapid transport of charge carriers. When exposed to visible light, the Bi_2WO_6 nanosheets were excited to create electrons and holes. The electrons on the conduction band (CB) of Bi_2WO_6 could not reduce O_2 to yield $\bullet O_2^-$ radicals. By contrast, the holes on the valence band (VB) of Bi_2WO_6 were positive enough to oxidize OH^- and generate •OH radicals, which were verified by trapping experiments (Figure 9). As a consequence, the holes and •OH radicals were engaged in the effective elimination of pollutants.

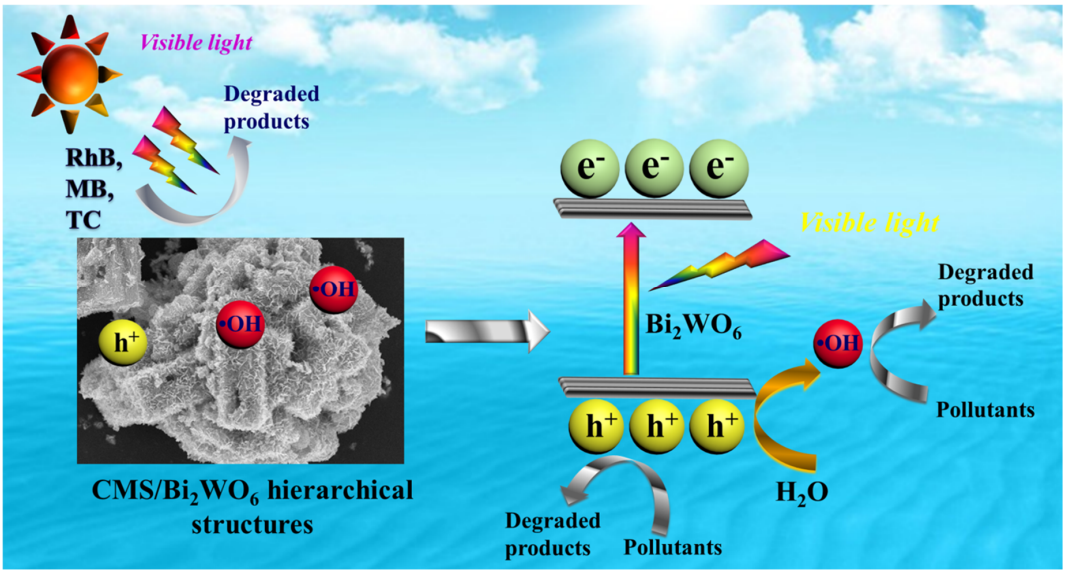

Figure 10. Proposed photocatalytic mechanism of the CMS/BWO composite photocatalyst.

3. Materials and Methods

3.1. Chemicals

All reagents of analytical grade were obtained from Chinese Sinopharm (Sinopharm, Beijing, China).

3.2. Photocatalysts Fabrication

Mussel shells dumped from factories in Zhoushan (Zhejiang, China) were collected and employed as raw materials. All chemicals were purchased from Chinese Sinopharm.

The mussel shells were first washed many times with deionized water to get rid of impurities, immersed in 0.5% HCl solution for 48 h, washed several times with deionized water, and then dried at 70 °C overnight. After that, the shells were smashed and sieved through a 600 mesh. Next, the obtained shell powders were placed in a muffle furnace and calcined at 700 °C for 3 h to obtain the calcined mussel shell (CMS).

Preparation of Bi_2WO_6/calcined mussel shell (CMS/BWO) composites: 0.5 mmol $Bi(NO_3)_3 \bullet 5H_2O$ and 0.25 mmol $Na_2WO_4 \bullet 2H_2O$ were dissolved in 20.0 mL ethylene glycol with the aid of sonication for 0.5 h, followed by the addition of 20 mL ethanol. Next, a certain amount of calcined mussel shell (CMS) was suspended in the above solution and stirred for 1 h. After that, the resultant suspension was put into a 50 mL Teflon-lined stainless steel autoclave and maintained at 150 °C for 30 h. Finally, the resultant x-CMS/BWO (x means the mass ratio of CMS to Bi_2WO_6, x = 4%, 8%, and 12%) was washed with deionized water and ethanol several times to get the CMS/BWO composites.

The characterization, photocatalytic tests, and determination of reactive species section are presented in the Supplementary Materials.

4. Conclusions

Bi_2WO_6/calcined mussel shell (CMS/BWO) composite photocatalysts have been constructed with a simple strategy. The as-fabricated CMS/BWO composite photocatalyst showed the hierarchical superstructures constructed by numerous Bi_2WO_6 2D nanosheets and CMS nanoflakes. Compared to the stacked Bi_2WO_6, the CMS/BWO composite presented plenty of exposed edges and open diffusion pathways, creating abundant open space and active sites for pollutant degradation. Consequently, CMS/BWO exhibited a remarkably enhanced photocatalytic capability towards RhB degradation. This composite photocatalyst had good stability and reusability. With •OH and h^+ as the pivotal active species, this photocatalyst was capable of efficiently decomposing and mineralizing toxic organic pollutants, manifesting a huge potential for the actual application. In addition, the integration of abandoned mussel shells with Bi_2WO_6 could effectively lower the cost of the photocatalysts, realizing the control of waste via a facile strategy, and stimulating interest for the future exploration of effective mussel shell-based photocatalysts for environmental purification.

Supplementary Materials: The following are available online at http://www.mdpi.com/2073-4344/10/10/1166/s1: The details about characterization methods, photocatalytic tests, and determination of reactive species section. Table S1: BET surface areas of as-fabricated catalysts.

Author Contributions: Conceptualization, S.L.; Formal analysis, B.X. and J.C.; Funding acquisition, S.L. and Y.L. (Yanping Liu); Project administration, C.W. and Y.L. (Yanping Liu); Resources, Y.L. (Yanping Liu), H.W. and Y.L. (Yu Liu); Validation, C.W., B.X. and J.C.; Writing—original draft, S.L.; Writing—review & editing, S.L. and Y.L. (Yanping Liu). All authors have read and agreed to the published version of the manuscript.

Funding: This work has been financially supported by the Science and Technology Project of Zhoushan (2017C41006, 2020C43001), the Public Projects of Zhejiang Province (LGN18E080003), the Fundamental Research Funds for Zhejiang Provincial Universities and Research Institutes (2019JZ00009), the Natural Science Foundation of Zhejiang Province (LY20E080014), and the National Natural Science Foundation of China (51708504).

Conflicts of Interest: The authors declare no conflict of interest.

References

1. Ma, D.; Li, Z.; Zhu, J.; Zhou, Y.; Chen, L.; Mai, X.; Liufu, M.; Wu, Y.; Li, Y. Inverse and highly selective separation of CO_2/C_2H_2 on a thulium–organic framework. *J. Mater. Chem. A* **2020**, *8*, 11933. [CrossRef]
2. Solís, R.R.; Rivas, J.; Chávez, A.M.; Dionysiou, D.D. Peroxymonosulfate/solar radiation process for the removal of aqueous microcontaminants. Kinetic modeling, influence of variables and matrix constituents. *J. Hazard. Mater.* **2020**, *400*, 123118. [CrossRef]
3. Xu, G.; Zhang, L.; Yu, W.; Sun, Z.; Guan, J.; Zhang, J.; Lin, J.; Zhou, J.; Fan, J.; Murugadoss, V.; et al. Low optical dosage heating-reduced viscosity for fast and large-scale cleanup of spilled crude oil by reduced graphene oxide melamine nanocomposite adsorbents. *Nanotechnology* **2020**, *31*, 225402. [CrossRef] [PubMed]
4. Chen, X.; Mao, S.S. Titanium dioxide nanomaterials: Synthesis, properties, modifications, and applications. *Chem. Rev.* **2007**, *107*, 2891–2959. [CrossRef] [PubMed]
5. Shi, Z.; Zhang, Y.; Shen, X.; Duoerkun, G.; Zhu, B.; Zhang, L.; Li, M.; Chen, Z. Fabrication of g-C_3N_4/BiOBr heterojunctions on carbon fibers as weaveable photocatalyst for degrading tetracycline hydrochloride under visible light. *Chem. Eng. J.* **2020**, *386*, 124010. [CrossRef]
6. Chang, F.; Wu, F.; Zheng, J.; Cheng, W.; Yan, W.; Deng, B.; Hu, X. In-situ establishment of binary composites a-$Fe_2O_3/Bi_{12}O_{17}Cl_2$ with both photocatalytic and photo-Fenton features. *Chemosphere* **2018**, *210*, 257–266. [CrossRef] [PubMed]
7. Pei, L.; Yuan, Y.; Zhong, J.; Li, T.; Yang, T.; Yan, S.; Ji, Z.; Zou, Z. Ta_3N_5 nanorods encapsulated into 3D hydrangea-like MoS_2 for enhanced photocatalytic hydrogen evolution under visible light irradiation. *Dalton Trans.* **2019**, *48*, 13176–13183. [CrossRef] [PubMed]
8. Rodríguez-Padrón, D.; Luque, R.; Muñoz-Batista, M.J. Waste-derived Materials: Opportunities in Photocatalysis. *Top. Curr. Chem.* **2020**, *378*, 1–28.

9. Regulska, E.; Breczko, J.; Basa, A. Pristine and graphene-quantum-dots-decorated spinel nickel aluminate for water remediation from dyes and toxic pollutants. *Water* **2019**, *11*, 953. [CrossRef]
10. Bajorowicz, B.; Kobylański, M.P.; Gołąbiewska, A.; Nadolna, J.; Zaleska-Medynska, A.; Malankowska, A. Quantum dot-decorated semiconductor micro- and nanoparticles: A review of their synthesis, characterization and application in photocatalysis. *Adv. Colloid Interface Sci.* **2018**, *256*, 352–372. [CrossRef]
11. Li, S.; Xue, B.; Chen, J.; Liu, Y.; Zhang, J.; Wang, H.; Liu, J. Constructing a plasmonic p-n heterojunction photocatalyst of 3D $Ag/Ag_6Si_2O_7/Bi_2MoO_6$ for efficiently removing broad-spectrum antibiotics. *Sep. Purif. Technol.* **2021**, *254*, 117579. [CrossRef]
12. Li, S.; Hu, S.; Jiang, W.; Zhang, J.; Xu, K.; Wang, Z. In situ construction of WO_3 nanoparticles decorated Bi_2MoO_6 microspheres for boosting photocatalytic degradation of refractory pollutants. *J. Colloid Interface Sci.* **2019**, *556*, 335–344. [CrossRef] [PubMed]
13. Li, S.; Hu, S.; Jiang, W.; Zhou, Y.; Liu, J.; Wang, Z. Facile synthesis of cerium oxide nanoparticles decorated flower-like bismuth molybdate for enhanced photocatalytic activity toward organic pollutant degradation. *J. Colloid Interface Sci.* **2018**, *530*, 171–178. [CrossRef] [PubMed]
14. Yu, X.; Huang, J.; Zhao, J.; Liu, S.; Xiang, D.; Tang, Y.; Li, J.; Guo, Q.; Ma, X.; Zhao, J. Efficient visible light photocatalytic antibiotic elimination performance induced by nanostructured $Ag/AgCl@Ti^{3+}$-TiO_2 mesocrystals. *Chem. Eng. J.* **2021**, *403*, 126359. [CrossRef]
15. Yu, X.; Zhao, J.; Huang, J.; Zhao, J.; Guo, Y.; Tang, Y.; Ma, X.; Li, Z.; Guo, Q.; Zhao, J. Visible light photocatalysis of amorphous Cl-Ta_2O_{5-x} microspheres for stabilized hydrogen generation. *J. Colloid Interface Sci.* **2020**, *572*, 141–150. [CrossRef] [PubMed]
16. Tang, Y.; Huang, J.; Jiang, M.; Yu, J.; Wang, Q.; Zhao, J.; Li, J.; Yu, X.; Zhao, J. Photo-induced synthesis of nanostructured Pt-on-Au/g-C_3N_4 composites for visible light photocatalytic hydrogen production. *J. Mater. Sci.* **2020**, *55*, 15574–15587. [CrossRef]
17. Guo, Q.; Zhao, J.; Yang, Y.; Huang, J.; Tang, Y.; Zhang, X.; Li, Z.; Yu, X.; Shen, J.; Zhao, J. Mesocrystalline Ta_3N_5 superstructures with long-lived charges for improved visible light photocatalytic hydrogen production. *J. Colloid Interface Sci.* **2020**, *560*, 359–368. [CrossRef]
18. Dai, C.; Liu, B. Conjugated polymers for visible-light-driven photocatalysis. *Energy Environ. Sci.* **2020**, *13*, 24–52. [CrossRef]
19. Hu, J.; Xie, J.; Jia, W.; Zhang, S.; Wang, S.; Wang, K.; Cao, Y. Interesting molecule adsorption strategy induced energy band tuning: Boosts 43 times photocatalytic Water splitting ability for commercial TiO_2. *Appl. Catal. B* **2020**, *268*, 118753. [CrossRef]
20. Zhao, Y.; Wang, Y.; Liu, E.; Fan, J.; Hu, X. Bi_2WO_6 nanoflowers: An efficient visible light photocatalytic activity for ceftriaxone sodium degradation. *Appl. Surf. Sci.* **2018**, *436*, 854–864. [CrossRef]
21. Zhang, H.; He, J.; Zhai, C.; Zhu, M. 2D Bi_2WO_6/MoS_2 as a new photo-activated carrier for boosting electrocatalytic methanol oxidation with visible light illumination. *Chin. Chem. Lett.* **2019**, *30*, 2338–2342. [CrossRef]
22. Zhang, L.S.; Wang, W.Z.; Zhou, L.; Xu, H.L. Bi_2WO_6 nano- and microstructures: Shape control and associated visible-light-driven photocatalytic activities. *Small* **2007**, *3*, 1618–1625. [CrossRef] [PubMed]
23. Zhang, N.; Ciriminna, R.; Pagliaro, M.; Xu, Y.-J. Nanochemistry-derived Bi_2WO_6 nanostructures: Towards production of sustainable chemicals and fuels induced by visible light. *Chem. Soc. Rev.* **2014**, *43*, 5276–5287. [CrossRef] [PubMed]
24. Etogo, A.; Liu, R.; Ren, J.B.; Qi, L.W.; Zheng, C.C.; Ning, J.Q.; Zhong, Y.J.; Hu, Y. Facile one-pot solvothermal preparation of Mo doped Bi_2WO_6 biscuit-like microstructures for visible-light-driven photocatalytic water oxidation. *Appl. Catal. B* **2016**, *4*, 13242–13250.
25. Zhou, S.; Zhang, C.; Liu, J.; Liao, J.; Kong, Y.; Xu, Y.; Chen, G. Oriented Bi_2WO_6 Photocatalyst induced by In Situ Bi Reduction towards Efficient Nitrogen Fixation. *Catal. Sci. Technol.* **2019**, *9*, 5562–5566. [CrossRef]
26. Wang, Y.; Jiang, W.; Luo, W.; Chen, X.; Zhu, Y. Ultrathin nanosheets g-C_3N_4@Bi_2WO_6 core-shell structure via low temperature reassembled strategy to promote photocatalytic activity. *Appl. Catal. B* **2018**, *237*, 633–640. [CrossRef]
27. Li, S.; Chen, J.; Hu, S.; Wang, H.; Jiang, W.; Chen, X. Facile construction of novel Bi_2WO_6/Ta_3N_5 Z-scheme heterojunction nanofibers for efficient degradation of harmful pharmaceutical pollutants. *Chem. Eng. J.* **2020**, *402*, 126165. [CrossRef]

28. Li, S.; Chen, J.; Hu, S.; Jiang, W.; Liu, Y.; Liu, J. A novel 3D Z-scheme heterojunction photocatalyst: $Ag_6Si_2O_7$ anchored on flower-like Bi_2WO_6 and its excellent photocatalytic performance for the degradation of toxic pharmaceutical antibiotics. *Inorg. Chem. Front.* **2020**, *7*, 529–541. [CrossRef]
29. Pei, L.; Li, T.; Yuan, Y.; Yang, T.; Zhong, J.; Ji, Z.; Yan, S.; Zou, Z. Schottky junction effect enhanced plasmonic photocatalysis by TaON@Ni NP heterostructures. *Chem. Commun.* **2019**, *55*, 11754–11757. [CrossRef]
30. Garrido-Rodriguez, B.; Cutillas-Barreiro, L.; Fernández-Calviño, D.; Arias-Estévez, M.; Fernández-Sanjurjo, M.J.; Álvarez-Rodríguez, E.; Núñez-Delgado, A. Competitive adsorption and transport of Cd, Cu, Ni and Zn in a mine soil amended with mussel shell. *Chemosphere* **2014**, *107*, 379–385. [CrossRef]
31. Wang, W.; Lin, F.; Yan, B.; Cheng, Z.; Chen, G.; Kuang, M.; Yang, C.; Hou, L. The role of seashell wastes in TiO_2/Seashell composites: Photocatalytic degradation of methylene blue dye under sunlight. *Environ. Res.* **2020**, *188*, 109831. [CrossRef] [PubMed]
32. Edralin, E.J.M.; Garcia, J.L.; dela Rosa, F.M.; Punzalan, E.R. Sonochemical synthesis, characterization and photocatalytic properties of hydroxyapatite nano-rods derived from mussel shells. *Mater. Lett.* **2017**, *196*, 33–36. [CrossRef]
33. Echabbi, F.; Hamlich, M.; Harkati, S.; Jouali, A.; Tahiri, S.; Lazar, S.; Lakhmiri, R.; Safi, M. Photocatalytic degradation of methylene blue by the use of titanium-doped Calcined Mussel Shells CMS/TiO_2. *J. Environ. Chem. Eng.* **2019**, *7*, 103293. [CrossRef]
34. Kaur, A.; Kansal, S.K. Bi_2WO_6 nanocuboids: An efficient visible light active photocatalyst for the degradation of levofloxacin drug in aqueous phase. *Chem. Eng. J.* **2016**, *302*, 194–203. [CrossRef]
35. Li, S.; Shen, X.; Liu, J.; Zhang, L. Synthesis of Ta_3N_5/Bi_2MoO_6 core-shell fiber-shaped heterojunctions as efficient and easily recyclable photocatalysts. *Environ. Sci. Nano* **2017**, *4*, 1155–1167. [CrossRef]